Ferromagnetic properties of the Mn-doped nanograined ZnO films

B. B. Straumal,[1,2,3,a)] S. G. Protasova,[2] A. A. Mazilkin,[2] A. A. Myatiev,[3] P. B. Straumal,[3,4] G. Schütz,[1] E. Goering,[1] and B. Baretzky[1,5]
[1]*Max-Planck-Institut für Metallforschung, Heisenbergstrasse 3, 70569 Stuttgart, Germany*
[2]*Institute of Solid State Physics, Russian Academy of Sciences, Chernogolovka, Moscow district 142432 Russia*
[3]*National University of Science and Technology, "Moscow Institute of Steel and Alloys—MISIS," Leninsky prospect 4, 119991 Moscow, Russia*
[4]*Institut für Materialphysik, Universität Münster, Wilhelm-Klemm-Str. 10, D-48149 Münster, Germany*
[5]*Karlsruher Institut für Technologie, Institut für Nanotechnologie, Hermann-von-Helmholtz-Platz 1, 76344 Eggenstein-Leopoldshafen, Germany*

(Received 26 February 2010; accepted 5 August 2010; published online 12 October 2010)

Dense nanograined pure and Mn-doped $Zn_{1-x}Mn_xO$ polycrystals with x ranging between 0.1–34 at. % were synthesized by the wet chemistry method from butanoate precursors. Pure and Mn-doped ZnO possesses ferromagnetic properties only if the ratio of grain boundary (GB) area to grain volume s_{GB} exceeds a certain threshold value s_{th}. The polycrystals in this work satisfy these conditions and, therefore, reveal ferromagnetic properties. The observed dependence of saturation magnetization on the Mn concentration shows an unexpected nonmonotonous behavior. The increase in saturation magnetization at low Mn concentration is explained by the injection of divalent Mn^{2+} ions and charge carriers into pure ZnO. The decrease in saturation magnetization between 0.1 and 5 at. % Mn can be explained by the increase in the portion of Mn^{3+} and Mn^{4+} ions. The second increase in saturation magnetization above 5 at. % Mn is explained by the formation of multilayer Mn segregation layer in ZnO GBs. The shape of the dependence of saturation magnetization on Mn concentration is different for the Mn-doped nanograined ZnO manufactured by different methods. It is most probably controlled by the topology of GB network (ferromagnetic GB foam) in the ZnO polycrystals. © *2010 American Institute of Physics*. [doi:10.1063/1.3486044]

I. INTRODUCTION

Dietl *et al.*[1] have theoretically predicted that ZnO doped by "magnetic" atoms like Co, Mn, or Fe possess ferromagnetic (FM) behavior with a high Curie temperature T_c above room temperature (RT). This is due to carrier-related FM interactions, where the FM ordering of the transition metal (TM) ions is induced by a magnetically polarized and doping modified ZnO host. Mn-doped ZnO is one of the most promising candidates for the application in spintronics among all diluted magnetic semiconductors (DMS) because Mn ions possess the highest magnetic moment along the 3*d* series. In addition, Mn posses a possible fully occupied majority 3*d* band, resulting in a stable fully spin polarized state. However, the experiments on FM in the Mn-doped ZnO leaded to the quite controversial results and are still debated in literature.[2–6] Understanding DMS remains one of the most important challenges in the condensed matter physics and physics of magnetism. In order to elucidate the dependence of RT ferromagnetism on the microstructure in ZnO, we have recently analyzed a large series of experimental publications with respect to the present specific grain boundary (GB) area, i.e., the ratio of GB area to grain volume s_{GB}.[7] FM only appears, if s_{GB} exceeds a certain threshold value s_{th}. Based on this important finding, nanograined pure and Mn-doped ZnO films have been prepared, which reveal reproducible RT-FM, where the magnetization is proportional to the film thickness, even for pure ZnO films.[7] Our findings strongly have suggested that GBs and related vacancies are the intrinsic origin for RT ferromagnetism. However, the (far from trivial) TM concentration dependence of saturation magnetization in Mn-doped ZnO has been not discussed by us so far.[7]

In this work we analyze the influence of Mn on the saturation magnetization of ZnO in a broad interval of Mn concentrations. We also try to explain the strongly nonmonotonous character of the magnetization dependence on Mn content.

II. EXPERIMENT

Pure and Mn-doped ZnO thin films consisting of dense equiaxial nanograins were produced by using the novel method of liquid ceramics.[8] The zinc (II) butanoate diluted in the organic solvent with zinc concentrations between 1 and 4 kg/m^3 was used as a precursor for the preparation of pure ZnO films. For the ZnO films doped with 0.1, 1, 4, 5, 6, 10, 16, 19, 20, 30, and 34 at. % Mn, zinc (II) butanoate solution was mixed with the manganese (III) butanoate solution in respective proportions. The butanoate precursor was deposited onto polycrystalline Al foils and on the (102) oriented sapphire single crystals. Drying at 100 °C in air (about 30 min) was followed by thermal pyrolysis in an electrical furnace (in air) at 550 °C. Similar method was recently proposed for zinc oleates.[9] The Zn and Mn content in doped oxides was measured by atomic absorption spectroscopy in a

a)Electronic mail: straumal@mf.mpg.de.

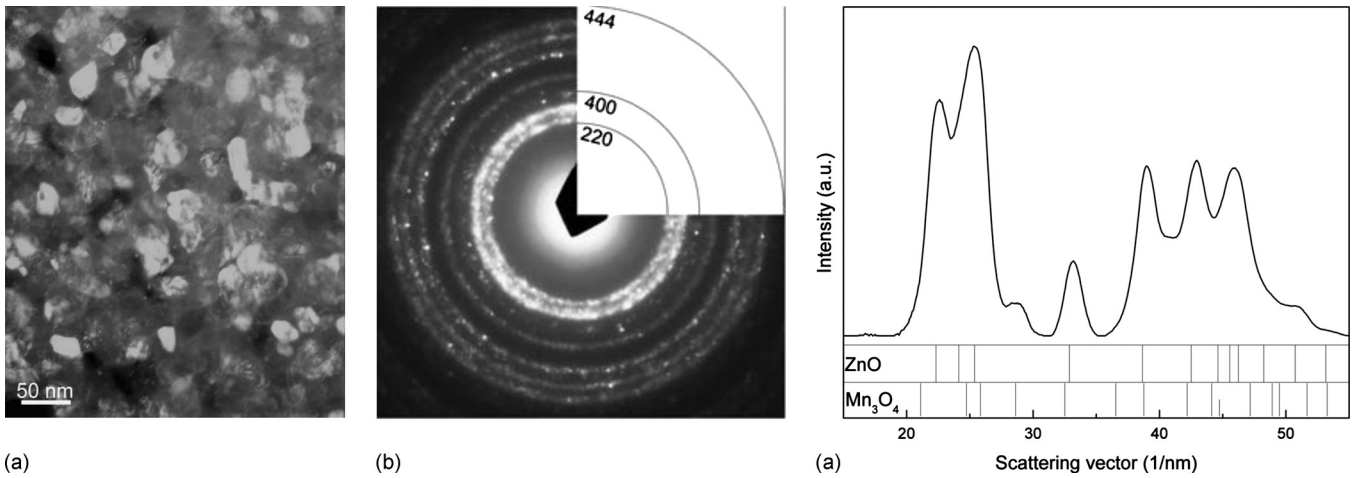

FIG. 1. (a) Dark field TEM micrograph of the nanograined ZnO+30 at. % Mn thin film deposited on Al foil by using the liquid ceramics method. (b) Selected area electron diffraction (SAED) pattern. No texture is visible, the rings for the ZnO wurtzite structure are present, three week rings for the Mn_3O_4 are also visible and marked in the white quadrant. Light spots are originated from the Al substrate. (c) Measured radial distribution of the SAED pattern intensity vs scattering vector $k=2\pi/d$ with the positions of diffraction lines for the ZnO and Mn_3O_4 (vertical lines in the bottom part).

Perkin-Elmer spectrometer and electron-probe microanalysis (EPMA). The presence of other magnetic impurities as Fe, Co, and Ni was below 0.001 at. %. During the thorough preparation procedure all possible precautions were taken to exclude any additional FM contaminations (nonmagnetic tweezers, ceramic scissors etc.). It is known from the literature[10] that the effect of contaminated substrate can completely conceal (hide) the FM signal of ZnO itself. We carefully measured the magnetization curves for bare Al and sapphire substrates and subtracted them from data for the substrates incl. ZnO films. The films were transparent and sometimes with a very slight greenish furnish with thicknesses between 50 and 900 nm. The thickness was determined by means of EPMA and edge-on transmission electron microscopy (TEM). EPMA investigations were carried out in a Tescan Vega TS5130 MM microscope equipped by the LINK energy-dispersive spectrometer produced by Oxford Instruments. TEM investigations were carried out on a Jeol JEM–4000FX microscope at an accelerating voltage of 400 kV. X-ray diffraction (XRD) data were obtained on a Siemens diffractometer (Fe $K\alpha$ radiation). Evaluation of the grain or particle size (D) from the x-ray peak broadening was performed using the so-called Williamson–Hall approach. In this approach experimental x-ray peak broadening is given as $\beta=0.9\lambda/D\cos\theta+4\varepsilon\sin\theta/\cos\theta$, where λ is the x-ray wavelength, θ is the diffraction angle, ε is the lattice strain, and β is the full-width at half maximum of the diffraction line.[11] The magnetic properties were measured on a superconducting quantum interference device (Quantum Design MPMS-7 and MPMS-XL). The magnetic field was applied parallel to the sample plane (in plane). The diamagnetic background signals, generated by the sample holder and the substrate, were carefully subtracted, due to the small absolute magnetic moments measured in the range of 10^{-6} to 10^{-4} emu.

III. RESULTS

Thin nanocrystalline and dense films of pure and Mn-doped ZnO, consisting of equiaxial grains with a mean grain size of about 15–25 nm were obtained [see dark field TEM micrograph in Fig. 1(a)]. In addition to TEM, selected area diffraction [Fig. 1(b)] and XRD were performed on thin film samples, which only showed signals from the ZnO wurtzite structure and the respective substrate for the 0.1, 1, 4, 5, 6, 10, 16, 19, and 20 at. % Mn. In samples with high Mn content of 30 and 34 at. % the second phase Mn_3O_4 with cubic lattice appears [Figs. 1(b) and 1(c) and Ref. 12]. The diffraction rings [Fig. 1(b)] were uniform and no texture could be observed.

The observed FM behavior in pure and doped nanocrystalline as well as dense ZnO films with 10 and 13 at. % Mn is depicted in Fig. 2. It clearly shows the pronounced FM indicated by the saturation of magnetization (above the applied field ~2 T) and hysteretic behavior (see insets). These magnetization and coercivity values are close to those obtained by other methods for Mn-doped samples.[13–18]

Saturation magnetization depends nonmonotonously on the Mn concentration (Fig. 3). It increases about three times by the addition of a very small amount of 0.1 at. % Mn to the pure ZnO. The magnetization drops down at further increase in Mn concentration and becomes almost nondistinguishable from the background around 5 at. % Mn. Above 5 at. % Mn the magnetization increases again. The saturation magnetization falls back to the background values only around 30 at. % Mn when the second phase Mn_3O_4 appears in the films in addition to the ZnO-based solid solution.

IV. DISCUSSION

A. Topology of the "FM GB foam" in the ZnO polycrystals

Recently we introduced the concept of the FM GB foam in pure and doped ZnO.[7] Based on the analysis of a multitude of experimental publications, we found that the values for the GB area to grain volume ratio s_{GB} is critical for the presence of ferromagnetism in pure and doped ZnO. Namely, FM only appears, if s_{GB} exceeds a certain threshold value s_{th}. For Mn-doped ZnO, $s_{th}=(2\pm4)\times10^5$ m^2/m^3, while the

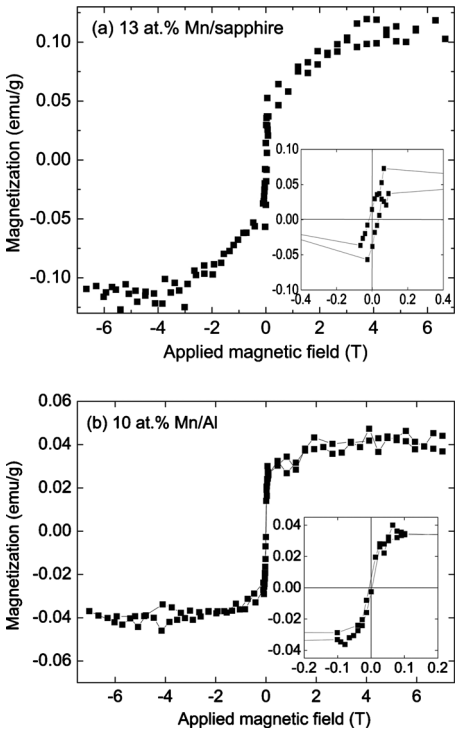

FIG. 2. Magnetization (calibrated in emu/g) at RT for ZnO thin films doped with 13 at. % Mn deposited on the sapphire substrate (a) and 10 at. % Mn deposited on the aluminum foil (b). The curves were obtained after subtracting the magnetic contribution from the substrate and the sample holder. Insets show the RT magnetic hysteresis. Only the enlarged central part of magnetization curves is given in order to clearly show the coercivity values.

threshold value for pure ZnO, $s_{th}=(5\pm3)\times10^7$ m^2/m^3 is more than two orders of magnitude higher.[7] However, the dependence of saturation magnetization on Mn concentration in ZnO was not discussed in Ref. 7.

In Fig. 4 the dependences of saturation magnetization on Mn concentration in ZnO samples obtained by different methods are shown. They were extracted from published experimental papers.[14,19–31] The magnetization measurements performed on the MnO single crystals or coarse-grained polycrystals with $s_{GB}<s_{th}$ did not reveal FM properties.[19–22] They are shown in Fig. 4(c) as having zero saturation magnetization. These nonmagnetic samples were grown by the hydrothermal method (+) (Ref. 23) or synthesized by chemical "pyrophoric reaction process" (∗),[19] sintering of conventional powders (♦),[21,22] (×),[20,23] or deposited as epitaxial single crystalline films (+).[24]

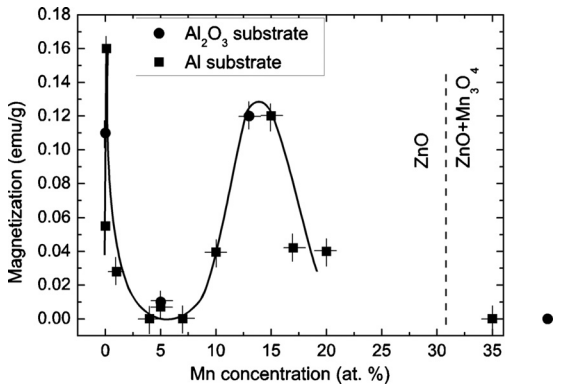

FIG. 3. Dependence of the saturation magnetization on the Mn concentration in ZnO nanograined polycrystals obtained by the "liquid ceramics" method.

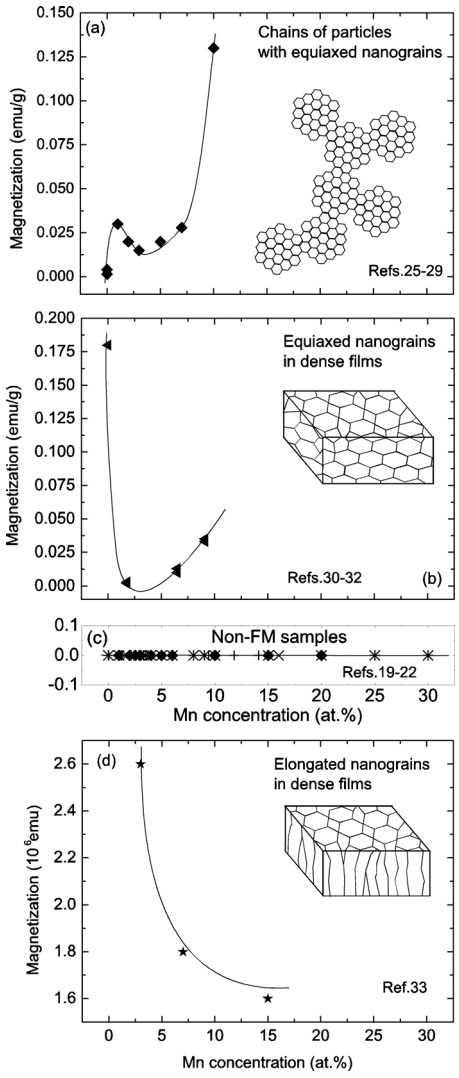

FIG. 4. Dependence of the saturation magnetization on the Mn concentration in ZnO obtained by other methods (Refs. 14 and 19–32) like hydrothermal method (+) (Ref. 23), chemical pyrophoric reaction process (∗) (Ref. 19), sintering of conventional or nanopowders (♦) (Refs. 21, 22, and 25–29), (×) (Refs. 20 and 23), deposition of epitaxial single crystalline films (+) (Ref. 24), pulsed laser deposition (◀) (Refs. 14, 30, and 31), and spray pyrolysis (★) (Ref. 32).

In Fig. 4(a) the concentration dependence is shown for the agglomerates of nanoparticles which consist of equiaxed ZnO nanograins obtained by the wet chemistry methods (♦).[25–29] Similar to Fig. 3, this dependence is nonmonotonous. When first portions of Mn (1 at. %) are added to the pure ZnO, the magnetization increases from 0.0014 to 0.03 emu/g. Between 1 and 3 at. % Mn the magnetization decreases to 0.014 emu/g and then increases again up to 0.13 emu/g at 10 at. % Mn.

In Fig. 4(b) the concentration dependence of saturation magnetization is shown for dense films with equiaxed nanograins obtained by the pulsed laser deposition (◀).[14,30,31] The dependence is also nonmonotonous and has a minimum of 0.002 emu/g at 1.8 at. % Mn. The magnetization decreases

from 0.18 emu/g in the pure ZnO with increasing Mn content. Above 1.8 at. % Mn the magnetization increases again up to 0.035 emu/g at 9.1 at. % Mn.

In Fig. 4(d) the concentration dependence of saturation magnetization is shown for the dense films with elongated nanograins obtained by the spray pyrolysis (★).[32] The Ref. 32 does not contain the information about the sample mass. Therefore, the magnetization values are given in emu. Magnetization decreases from 2.6×10^{-6} emu at 3 at. % Mn to 1.6×10^{-6} emu at 15 at. % Mn.

All samples shown in Figs. 4(a), 4(b), and 4(d) possessing FM properties have grain size below 100 nm and are, therefore, two orders of magnitude s_{GB} above critical value s_{th} for the Mn-doped ZnO.[7] We supposed that ferromagnetism in pure and doped ZnO appears due to the defects positioned in the GBs. GBs form, therefore, a kind of "FM foam" in the ZnO polycrystals.[7] If the cells of a "GB foam" are too large, effective exchange coupling strength is too small and ferromagnetism cannot appear. However, we did not discuss the possible influence of the topology of a GB foam.[7] In the samples studied in this work (Fig. 3) and those represented in Fig. 4 the spatial distribution and shape of GBs as well as topology of a GB network in the material are different. This leads to different shapes of the concentration dependency of the saturation magnetization, though all of them have a pronounced minimum at medium Mn concentrations. What is the reason of nonmonotonous dependences of saturation magnetization?

B. Nonmonotonous dependence of the saturation magnetization on Mn concentration

Why the saturation magnetization of FM nanograined ZnO behaves so nonmonotonically with increasing Mn content? Namely (Fig. 3),

- the magnetization increases almost three times by the addition of a very small amount of 0.1 at. % Mn to the pure ZnO;
- the magnetization drops down at further increase in Mn concentration and becomes almost nondistinguishable from the background around 5 at. % Mn;
- above 5 at. % Mn the magnetization increases again;
- it falls back to the background values only around 30 at. % Mn, when a second phase of Mn_3O_4 appears in the films in addition to the ZnO-based solid solution.

The introduction of the first portions of Mn injects the Mn^{2+} ions into wurtzite lattice of ZnO and drastically increases the magnetization value comparing with the pure ZnO (Fig. 3). Similar strong increase in the magnetization from 0.015 to 0.08 to emu/g was observed between 0.01 and 0.08 at. % Mn in the ZnO thin films.[33] These films were grown on glass substrates using reactive magnetron sputtering [elongated grains, similar to Fig. 4(d)] and were additionally doped by 0.05 at. % Li. Dietl with co-workers have already theoretically predicted that ZnO doped by magnetic atoms like Co, Mn, or Fe would possess FM behavior with a high Curie temperature T_c.[1] Their idea was that it is due to carrier-related FM interactions, where the FM ordering of the TM ions is induced by a magnetically polarized and by doping modified ZnO host. Later the FM behavior was indeed found in Mn- and Co-doped ZnO, however, the reasons for it are more complicated.[7]

The Raman-scattering experiments on the Mn-doped ZnO cornlike nanorods demonstrated that compared with the vibration modes of ZnO powder, two additional vibration modes were observed at about 521–528 cm^{-1} and 642–648 cm^{-1} in the Raman spectrum of the Mn-doped ZnO.[34] The vibration mode at 522 cm^{-1} could be associated with Mn doping because the ionic radius of Mn^{2+} (0.66 Å) is larger than that of Zn^{2+} (0.60 Å).[35] Therefore, when Mn^{2+} ions occupied the Zn sites, the lattice defects were introduced or intrinsic host-lattice defects were activated. Therefore, additional vibration modes could appear after Mn doping of ZnO.

The near-edge x-ray absorption fine structure (NEXAFS) measurements at the O *K*-edge clearly exhibited a pre-edge spectral feature,[36] which evolved with Mn doping, similar to one observed in hole-doped cuprates and manganites.[37–39] Below certain concentration of Mn such pre-edge spectral feature at the O *K*-edge disappears.[40] The observed pre-edge spectral feature originates with Mn doping and is ascribed to dipole transitions from O $1s$ to O $2p$ states that are hybridized with the unoccupied states of Mn $3d$. Therefore, the intensity of this peak represents the Mn $3d$ density of states and the continuous increase in this peak with Mn doping indicates more unoccupied states at the Mn $3d$ levels and, hence, reflects the presence of more charge carriers.[36]

The decrease in the saturation magnetization between 0.1 and 5 at. % Mn (Figs. 3 and 4) can be explained by the appearance of Mn^{3+} and Mn^{4+} in addition to the Mn^{2+} ions. The electron paramagnetic resonance (EPR) was used to probe the valence state of the Mn atoms in the Mn-doped ZnO-nanowires obtained by the precipitation from the Zn acetate and Mn oleate solution in trioctylamine.[41] EPR spectra changed around 1 at. % Mn. Below 1 at. % Mn doping, the EPR spectrum contained two contributions: (i) a broad resonance resulting from antiferromagnetic interactions of Mn^{2+} ions and (ii) a sextuplet from isolated spins. Due to its half-filled d shell ($3d^5$) with spin $S=5/2$ and angular momentum $L=0$ and the 100% prevalent ^{55}Mn nucleus spin $I=5/2$, the resonance of an isolated Mn^{2+} ion located substitutionally on a Zn site in hexagonal ZnO should result in a sextuplet. This sextuplet disappeared above 1 at. % Mn, and only a broad signal was measured. In Ref. 34 the Mn-doped ZnO cornlike nanorods were obtained by the rheological phase reaction-precursor method. The thermal decomposition of the precursors was performed at 450 °C for 2 h in air. The grain size was about 10 nm, the grains were equiaxial, and the grain structure of polycrystalline cornlike rods was almost poreless. The EPR sextuplet from the isolated Mn^{2+} ions weakened by increase in Mn content from 3 to 7 at. %.

The valence bond of Mn was also investigated using x-ray photoelectron spectroscopy (XPS).[34] Overlapping bands were deconvoluted into separated peaks by Gauss fitting. It has been found that there are three peaks at 640.40 eV, 641.40 eV, and 642.65 eV attributed to Mn^{2+}, Mn^{3+}, and Mn^{4+}, respectively.[42] With increase in Mn concentration

from 3 to 7 at. % the input of Mn^{2+} ions decreased and the area of Mn^{3+} and Mn^{4+} peaks increased. However, the change in the XPS-line shape can also be related by the increase in metallic conductivity and the correlated asymmetric photoemission line shape.[43]

The Mn $L_{3,2}$-edge NEXAFS spectra determine the 3*d* occupancy of the Mn ions and, hence, provide direct information on the valence states of the Mn ions in the compounds.[36] As the valence changes from Mn^{2+}, Mn^{3+}, and Mn^{4+} states, the NEXAFS at the L_3-edge shows a shift toward the higher energy side and the spectral shape changes significantly with the number of 3*d* electrons.[44,45] The ZnO and Mn-doped ZnO thin films with 3, 5, 7, 10, and 15 at. % Mn were deposited on Si(100) by using a spray pyrolysis technique.[36] The peak at 640 eV in the Mn $L_{3,2}$-edge NEXAFS spectra was attributed to Mn^{2+} state and the higher energy features were attributed to the mixed valence states of Mn^{2+} with Mn^{3+}/Mn^{4+}. This behavior was also supported by Mn *K*-edge spectra.[36]

Repeated increase in the magnetization above 5 at. % Mn can be driven by the formation of multilayer Mn segregation in ZnO GBs (GB phases). We observed that the accumulation of Mn in GBs and free surfaces drastically shifts the line of Mn solubility limit in ZnO to the higher Mn concentrations.[12] For example, at 550 °C the total solubility in the bulk is about 10 at. % Mn and in the nanograined sample with grain size below 20 nm it is about 40 at. % Mn. Simple estimation demonstrated that this shift is only possible when Mn forms a multilayer GB segregation (up to 10 monolaeyrs of Mn). Such layers of a GB phase of a finite thickness of few nm were first observed and theoretically treated with the aid of force-balance models in the pioneering works of Clarke on silicon nitride.[46–49] Later, nanometer thick, disordered GB films of a nearly constant or "equilibrium" thickness have been widely observed in ZnO doped by Bi_2O_3.[50–55] ZnO doped by Bi is used for varistors manufacturing. Varistors exhibit highly nonlinear current–voltage characteristics with a high resistivity below a threshold electric field, becoming conductive when this field is exceeded. This phenomenon enables them to be used in current oversurge protection circuits.[55] After liquid-phase sintering, such material consists of ZnO grains separated by thin Bi_2O_3-rich GB layers.

We suppose that above 5 at. % Mn such segregation layer forms in the ZnO GBs, its thickness increases with increasing Mn content and reaches about ten monolayers at the solubility limit of Mn in our nanograined films.[12] This fact leads to the repeated increase in the saturation magnetization between 5 and 20 at. % Zn.

Above 25–28 at. % Mn the second phase Mn_3O_4 with cubic lattice appears in the samples in addition to the ZnO wurtzite phase.[12] We concluded that in the FM ZnO the crystalline ZnO grains are nonmagnetic and surrounded by a FM foamlike GB network.[7] The appearance of the Mn_3O_4 most probably destroys this GB foam and results in the decrease in the magnetization to the background values.

Thus, the concentration dependence of the saturation magnetization in Mn-doped nanograined ZnO is principally nonmonotonous. First of all, as we have shown before,[7] the presence of critical amount of GBs is the condition for the existence of FM behavior in ZnO. If the amount of GBs is high enough [above $s_{th}=(5\pm3)\times10^7$ m^2/m^3] the FM behavior appears even without doping by the magnetic atoms like Mn or Co.[7] If the amount of GBs is below the threshold value [$s_{th}=(2\pm4)\times10^5$ m^2/m^3 for Mn-doped ZnO],[7] ferromagnetism cannot be observed also with the help of Mn doping [Fig. 4(c)].

However, the comparison of Fig. 3 and the data taken from the literature [Figs. 4(a), 4(b), and 4(d)] demonstrates that the position of minima and maxima on the concentration dependence of the saturation magnetization is very sensitive to the morphology of GB network (Fig. 4) and to the oxygen content.[56] Rather low values of saturation magnetization and the necessity of a critical GB amount for the FM behavior of ZnO allow us to draw the conclusion that ZnO is inhomogeneous and consists of the network of FM GB layers and non-FM grains. Theoretic calculations for the behavior of such inhomogeneous media containing both magnetic and nonmagnetic volumes were performed recently.[57,58] The results of theoretic modeling show that in such media two percolation thresholds exist with increasing amount of nonmagnetic phase. At low amount of nonmagnetic phase the nonmagnetic volumes (clusters) are isolated and interspersed into the magnetic phase. First percolation threshold appears when the nonmagnetic volumes become connected. Second percolation threshold corresponds to the situation when bridges between magnetic volumes break and magnetic clusters becomes isolated.[57,58] Most probably the FM ZnO is situated somewhere between those percolation thresholds. The presence of Mn ions with different valence states (Mn^{2+}, Mn^{3+}, and Mn^{4+}) (Ref. 59) causes the nonmonotonous behavior. The art and topology of the connections between FM GB layers [see schemes in Figs. 4(a), 4(b), and 4(d)] changes the positions of minima and maxima of the saturation magnetization (Fig. 4).

V. CONCLUSIONS

Pure and Mn-doped ZnO possesses FM properties only if the ratio of GB area to grain volume exceeds a certain threshold value s_{th}. For Mn-doped ZnO s_{th} is higher than that for the pure ZnO (2×10^5 m^2/m^3 and $5\pm\times10^7$ m^2/m^3, respectively). The dependence of saturation magnetization on Mn concentration is very nonmonotonous. The increase in saturation magnetization at low Mn concentration is due to the injection of divalent Mn^{2+} ions and charge carriers into pure ZnO. The decrease in saturation magnetization between 0.1 and 5 at. % Mn is due to the increase in the portion of Mn^{3+} and Mn^{4+} ions. The second increase in saturation magnetization above 5 at. % Mn is due to the formation of multilayer Mn segregation layer in ZnO GBs. The shape of dependence of saturation magnetization on Mn concentration is different for the Mn-doped nanograined ZnO manufactured by different methods. It depends on the topology of GB network (FM GB foam) in the ZnO polycrystals.

ACKNOWLDGEMENTS

The authors would like to thank the Russian Foundation for Basic Research (Contract Nos. 10-02-00086 and 09-02-90469), the Deutsche akademische Austauschdienst (DAAD) "MISiS," and the Programme of Creation and Development of the National University of Science and Technology for their financial support to these investigations and relating travel. The authors also cordially thank Professor A. Murtazaev, Dr. D. Goll, Dr. A. Nekrasov, Ms. Th. Dragon, Ms. M. Kelsch, and Ms. U. Salzberger.

[1]T. Dietl, H. Ohno, F. Matsukura, J. Cibert, and D. Ferrand, Science **287**, 1019 (2000).
[2]M. Lafkioti, E. Goering, S. Gold, G. Schuetz, S. N. Barilo, S. V. Shiryaev, G. L. Bychkov, P. Lemmens, V. Hinkov, J. Deisenhofer, and A. Loidl, Nat. Phys. **10**, 123030 (2008).
[3]G. Mayer, M. Fonin, S. Voss, U. Rüdiger, and E. Goering, IEEE Trans. Magn. **44**, 2700 (2008).
[4]N. Grumbach, A. Barla, L. Joly, B. Donnio, G. Rogez, E. Terazzi, J.-P. Kappler, and J.-L. Gallani, Eur. Phys. J. B **73**, 103 (2010).
[5]N. H. Hong, A. Barla, J. Sakai, and N. Q. Huong, Phys. Status Solidi C **4**, 4461 (2007).
[6]A. Ney, K. Ollefs, T. Kammermeier, V. Ney, T. C. Kaspar, S. A. Chambers, F. Wilhelm, and A. Rogalev, Phys. Rev. Lett. **100**, 157201 (2008).
[7]B. B. Straumal, A. A. Mazilkin, S. G. Protasova, A. A. Myatiev, P. B. Straumal, G. Schütz, P. A. van Aken, E. Goering, and B. Baretzky, Phys. Rev. B **79**, 205206 (2009).
[8]B. B. Straumal, A. A. Mazilkin, S. G. Protasova, A. A. Myatiev, P. B. Straumal, and B. Baretzky, Acta Mater. **56**, 6246 (2008).
[9]W. S. Chiu, P. S. Khiew, D. Isa, M. Cloke, S. Radiman, R. Abd-Shukor, M. H. Abdullah, and N. M. Huang, Chem. Eng. J. **142**, 337 (2008).
[10]Y. Belghazi, G. Schmerber, S. Colis, J. L. Rehspringer, and A. Dinia, Appl. Phys. Lett. **89**, 122504 (2006).
[11]L. Lábár, Microsc. Microanal. **14**, 287 (2008).
[12]B. B. Straumal, B. Baretzky, A. A. Mazilkin, S. G. Protasova, A. A. Myatiev, and P. B. Straumal, J. Eur. Ceram. Soc. **29**, 1963 (2009).
[13]A. K. Pradhan, D. Hunter, K. Zhang, J. B. Dadson, S. Mohanty, T. M. Williams, K. Lord, R. R. Rakhimov, U. N. Roy, Y. Cui, A. Burger, J. Zhang, and D. J. Sellmyer, Appl. Surf. Sci. **252**, 1628 (2005).
[14]M. Diaconu, H. Schmidt, H. Hochmuth, M. Lorenz, G. Benndorf, D. Spemann, A. Setzer, P. Esquinazi, A. Pöppl, H. von Wenckstern, K.-W. Nielsen, R. Gross, H. Schmid, W. Mader, G. Wagner, and M. Grundmann, J. Magn. Magn. Mater. **307**, 212 (2006).
[15]K. C. Barick and D. Bahadur, J. Nanosci. Nanotechnol. **7**, 1935 (2007).
[16]K. Masuko, A. Ashida, T. Yoshimura, and N. Fujimura, J. Magn. Magn. Mater. **310**, e711 (2007).
[17]A. Che Mofor, A. El-Shaer, A. Bakin, H.-H. Wehmann, H. Ahlers, U. Siegner, S. Sievers, M. Albrecht, W. Schoch, N. Izyumskaya, V. Avrutin, J. Stoemenos, and A. Waag, Superlattices Microstruct. **39**, 381 (2006).
[18]S. W. Yoon, S.-B. Cho, S. C. We, S. Yoon, B. J. Suh, H. K. Song, and Y. J. Shin, J. Appl. Phys. **93**, 7879 (2003).
[19]S. K. Mandal, A. K. Das, T. K. Nath, D. Karmakar, and B. Satpati, J. Appl. Phys. **100**, 104315 (2006).
[20]S. Venkataraj, N. Ohashi, I. Sakaguchi, Y. Adachi, T. Ohgaki, H. Ryoken, and H. Haneda, J. Appl. Phys. **102**, 014905 (2007).
[21]J. Alaria, P. Turek, M. Bernard, M. Bouloudenine, A. Berbadj, N. Brihic, G. Schmerber, S. Colis, and A. Dinia, Chem. Phys. Lett. **415**, 337 (2005).
[22]S. Kolesnik and B. Dabrowski, J. Appl. Phys. **96**, 5379 (2004).
[23]M. H. Kane, W. E. Fenwick, M. Strassburg, B. Nemeth, R. Varatharajan, Q. Song, D. J. Keeble, H. El-Mkami, G. M. Smith, Z. J. Zhang, J. Nause, C. J. Summers, and I. T. Ferguson, Phys. Status Solidi B **244**, 1462 (2007).
[24]A. I. Savchuk, P. N. Gorley, V. V. Khomyak, K. S. Ulyanytsky, S. V. Bilichuk, A. Perrone, and P. I. Nikitin, Mater. Sci. Eng., B **109**, 196 (2004).
[25]G. Lawes, A. S. Risbud, A. P. Ramirez, and R. Seshadi, Phys. Rev. B **71**, 045201 (2005).
[26]O. D. Jayakumar, H. G. Salunke, R. M. Kadam, M. Mohapatra, G. Yaswant, and S. K. Kulshreshtha, Nanotechnology **17**, 1278 (2006).
[27]M. Pal and M. Pal, Jpn. J. Appl. Phys., Part 1 **44**, 7901 (2005).
[28]B. Babić-Stojić, D. Milivojević, J. Blanuša, V. Spasojević, N. Bibić, B. Simonović, and D. Aranđelović, J. Phys.: Condens. Matter **20**, 235217 (2008).
[29]Z. Yan, Y. Ma, D. Wang, J. Wang, Z. Gao, L. Wang, P. Yu, and T. Song, Appl. Phys. Lett. **92**, 081911 (2008).
[30]M. Diaconu, H. Schmidt, H. Hochmuth, M. Lorenz, G. Benndorf, J. Lenzner, D. Spemann, A. Setzer, K.-W. Nielsen, P. Esquinazi, and M. Grundmann, Thin Solid Films **486**, 117 (2005).
[31]Q. Xu, H. Schmidt, S. Zhou, K. Potzger, M. Helm, H. Hochmuth, M. Lorenz, A. Setzer, P. Esquinazi, C. Meinecke, and M. Grundmann, Appl. Phys. Lett. **92**, 082508 (2008).
[32]M. Subramanian, V. Selvaraj, P. Ilanchezhiyan, G. M. Kumar, R. Jayavel, and T. Soga, Jpn. J. Appl. Phys. **48**, 06FF07 (2009).
[33]C. W. Zou, H. J. Wang, M. L. Yi, M. Li, C. S. Liu, L. P. Guo, D. J. Fu, and T. W. Kang, Appl. Surf. Sci. **256**, 2453 (2010).
[34]C. J. Cong and K. L. Zhang, Phys. Status Solidi A **243**, 2764 (2006).
[35]L. W. Yang, X. L. Wu, G. S. Huang, T. Qiu, and Y. M. Yang, J. Appl. Phys. **97**, 014308 (2005).
[36]P. Thakur, K. H. Chae, J.-Y. Kim, M. Subramanian, R. Jayavel, and K. Asokan, Appl. Phys. Lett. **91**, 162503 (2007).
[37]P. Abbamonte, L. Venama, A. Rusydi, G. A. Sawatzky, G. Logvenov, and I. Bozovic, Science **297**, 581 (2002).
[38]E. Pellegrin, N. Nücker, J. Fink, S. L. Molodtsov, A. Gutierrez, E. Navas, O. Strebel, Z. Hu, M. Domke, G. Kaindl, S. Uchida, Y. Nakamura, J. Markl, M. Klauda, G. Saemann-Ischenko, A. Krol, J. L. Peng, Z. Y. Li, and R. L. Greene, Phys. Rev. B **47**, 3354 (1993).
[39]K. Asokan, J. C. Jan, K. V. R. Rao, J. W. Chiou, H. M. Tsai, S. Mookerjee, W. F. Pong, M.-H. Tsai, R. Kumar, S. Husain, and J. P. Shrivastava, J. Phys.: Condens. Matter **16**, 3791 (2004).
[40]J.-H. Guo, A. Gupta, P. Sharma, K. V. Rao, M. A. Marcus, C. L. Dong, J. M. O. Guillen, S. M. Butorin, M. Mattesini, P. A. Glans, K. E. Smith, C. L. Chang, and R. Ahuja, J. Phys.: Condens. Matter **19**, 172202 (2007).
[41]G. Clavel, N. Pinna, and D. Zitoun, Phys. Status Solidi A **204**, 118 (2007).
[42]J. F. Moulder, W. F. Stickle, P. E. Sobol, and K. D. Bomben, in *Handbook of X-Ray Photoelectron Spectroscopy*, 1st ed., edited by J. Chastain and P. C. Kling, Jr. (Physical Electronics, Inc., Eden Prairie, MN, 1995).
[43]S. Doniach and M. Sunjic, J. Phys. C **3**, 285 (1970).
[44]F. M. F. de Groot, J. C. Fuggle, B. T. Thole, and G. A. Sawatzky, Phys. Rev. B **42**, 5459 (1990).
[45]G. van der Laan and I. W. Kirkman, J. Phys.: Condens. Matter **4**, 4189 (1992).
[46]D. R. Clarke, J. Am. Ceram. Soc. **70**, 15 (1987).
[47]D. R. Clarke, T. M. Shaw, A. P. Philipse, and R. G. Horn, J. Am. Ceram. Soc. **76**, 1201 (1993).
[48]I. Tanaka, H.-J. Kleebe, M. K. Cinibulk, J. Bruley, D. R. Clarke, and M. J. Rühle, J. Am. Ceram. Soc. **77**, 911 (1994).
[49]M. Bobeth, D. R. Clarke, and W. Pompe, J. Am. Ceram. Soc. **82**, 1537 (1999).
[50]H. Wang and Y.-M. Chiang, J. Am. Ceram. Soc. **81**, 89 (1998).
[51]J. P. Gambino, W. D. Kingery, G. E. Pike, and H. R. Philipp, J. Am. Ceram. Soc. **72**, 642 (1989).
[52]E. Olsson and G. L. Dunlop, J. Appl. Phys. **66**, 3666 (1989).
[53]B. B. Straumal, A. A. Mazilkin, P. B. Straumal, and A. A. Myatiev, Int. J. Nanomanufact. **2**, 253 (2008).
[54]J. Luo and Y.-M. Chiang, Annu. Rev. Mater. Res. **38**, 227 (2008).
[55]H. Qian, J. Luo, and Y.-M. Chiang, Acta Mater. **56**, 862 (2008).
[56]A. Di Trolio, C. Veroli, A. M. Testa, and D. Fiorani, Superlattices Microstruct. **46**, 101 (2009).
[57]A. K. Murtazaev, A. B. Babaev, and G. Ya. Aznaurova, Solid State Phenom. **152–153**, 571 (2009).
[58]A. K. Murtazaev, A. B. Babaev, and G. Ya. Aznaurova, J. Exp. Theor. Phys. **109**, 442 (2009).
[59]P. Thakur, S. Gautam, K. H. Chae, M. Subramanain, R. Jayavel, and K. Asokan, J. Korean Phys. Soc. **55**, 177 (2009).